Integration of Remote Sensing and Crowdsourced Data for Fine-Grained Urban Flood Detection

Zhenjie Liu, *Member, IEEE*, Jun Li, *Fellow, IEEE*, Lizhe Wang, *Fellow, IEEE*, and Antonio Plaza, *Fellow, IEEE*

***Abstract*—In the context of frequent global flood disasters, flood detection is of great significance for emergency management and human sustainable development, especially in urban areas with increasing population and socio-economic activities. However, there are similar reflection/scattering characteristics between flooded and nonflooded land use and land cover (LULC) classes in complex urban environments, which limit the accurate detection of floods. In this study, we develop a new method for fine-grained and accurate flood detection by integrating multitemporal Sentinel-1 synthetic aperture radar images, OpenStreetMap data, and convolutional neural networks. We take the 2017 Houston flood event as a test case, where the study areas are divided into six fine-grained LULC classes, i.e., residential areas, service areas, main roads, forest, grassland, and waterways. Based on the information of fine-grained LULC classification, the proposed method performs more prominently than the baseline methods for urban flood detection. Specifically, compared with such baseline methods, F1 score, overall accuracy, and Kappa increase by more than 3.96%, 4.53%, and 9.26%, respectively. The integration of remote sensing and crowdsourced data provides a new perspective for flood detection in complex urban environments, thus supporting emergency management.**

***Index Terms*—Data fusion, flood detection, OpenStreetMap (OSM), Sentinel-1, supervised classification.**

I. Introduction

FREQUENT global floods have caused serious casualties and socio-economic losses, especially in urban areas with high population density and high proportion of impervious surface [1], [2]. The United Nations Office for Disaster Risk Reduction pointed out that the number of global flood disasters has increased dramatically from 1980–1999 (1389) to 2000–2019 (3254).[1] At present, many disaster prevention and mitigation measures taken by governments and relevant institutions and organizations in flood management have advanced significantly. However, due to global climate change and the increasing population and socio-economic activities in disaster-prone urban areas, the frequency and risk of urban flood disasters have soared simultaneously. In this context, urban flood disasters remain one of the key challenges of the 21st century [3], [4]. As a result, accurate urban flood detection is of great significance for emergency management, environmental protection, and human sustainable development.

Traditional ground surveys can collect accurate flood information on a local scale, but require to consider high costs and the threat to life caused by flood disasters. In contrast, remote sensing technology can monitor large-scale flood disasters and obtain near-real-time spatio–temporal information, which has been widely used in urban flood detection [5], [6], [7]. Common data sources mainly include optical remote sensing satellites and synthetic aperture radar (SAR) data. Optical data can capture reflectance differences of flooded areas in different spectral bands, but limited by factors, such as extreme weather and cloud cover during flood disasters [8]. Compared with optical remote sensing, SAR is capable to obtain all-weather and all-day information about floods. So far, a large number of studies have leveraged SAR data for urban flood detection [9], [10], [11]. However, few research studies have explored the SAR reflection/scattering mechanisms of fine-grained land use and land cover (LULC). In complex urban environment, different LULC classes generally exhibit various reflection/scattering mechanisms when flooding, such as specular reflection, surface backscatter, as well as single, double, and triple bounces [12], [13]. Meanwhile, intensive residential activities in urban areas also have an impact on SAR characteristics [14], [15]. In this case, a flooded LULC may have similar reflection/scattering characteristics than another nonflooded LULC, and ignoring this phenomenon is likely to reduce the performance of flood detection.

In addition to flood detection, remotely sensed data have also become one of the most important data sources for LULC classification [16], [17]. But these data may not be able to identify fine-grained LULC types with similar spectral, geometrical, and contextual features but different anthropogenic properties, such as residential areas and service areas. [18], [19]. With the development of mobile positioning and data acquisition techniques, crowdsourced data are voluntarily created to provide human activities and socio-economic information [20]. A number of crowdsourced LULC datasets have been developed using tools, such as OpenStreetMap (OSM), LandSense, and

Manuscript received 13 December 2023; revised 20 June 2024; accepted 20 July 2024. Date of publication 24 July 2024; date of current version 8 August 2024. This work was supported by the National Natural Science Foundation of China under Grant T2225019. *(Corresponding author: Jun Li.)*

Zhenjie Liu, Jun Li, and Lizhe Wang are with the Hubei Key Laboratory of Intelligent Geo-Information Processing, and School of Computer Science, China University of Geosciences, Wuhan 430078, China (e-mail: liuzhenjie@cug.edu.cn; lijuncug@cug.edu.cn; lizhe.wang@gmail.com).

Antonio Plaza is with the Hyperspectral Computing Laboratory Department of Technology of Computers and Communications, Escuela Politécnica, University of Extremadura, 06006 Badajoz, Spain (e-mail: aplaza@unex.es).

This article has supplementary downloadable material available at https://doi.org/10.1109/JSTARS.2024.3433010, provided by the authors.

Digital Object Identifier 10.1109/JSTARS.2024.3433010

[1][Online]. Available: https://www.undrr.org/publication/human-cost-disasters-2000-2019

Geopedia, among others [21], [22], [23]. In particular, OSM is a free, open-access, crowdsourced platform with which volunteers from all over the world collaboratively contribute geometric representations of LULC data [24]. OSM has great potential for fine-grained classification of urban LULC due to key factors, such as the availability of up-to-date data with global coverage, improvements in data quality over time, and extensive volume and variety of thematic attribute data [21], [25], [26]. However, the spatial coverage, temporal accuracy, positional accuracy, and thematic accuracy of OSM data are heterogeneous across different regions, especially for polygon vector data generated by individual users [27], [28]. In comparison, OSM line vector data are usually provided by governments, social organizations, and institutions, and exhibit advantages, such as comprehensive coverage, accurate land attributes, and spatio–temporal positioning, including road data [29], [30].

To address the problems introduced by the similar reflection/scattering characteristics between flooded and nonflooded LULCs in complex urban environments, we propose a new method for fine-grained flood detection based on the combination of OSM line vector data and multitemporal Sentinel-1 SAR images. The 2017 Houston (Texas) flood event is adopted as a test case to test the proposed method. The main innovative contributions of our work are as follows.

1) A systematic investigation of the reflection/scattering characteristics of different LULCs in complex urban environment.
2) Fine-grained LULC classification is carried out by using OSM line vector data.
3) A new method for fine-grained and accurate flood detection is developed based on LULC classification and Sentinel-1 SAR images.

The rest of this article is organized as follows. Section II introduces related works in the areas of LULC classification and urban flood detection. Section III describes the datasets and the newly proposed method in detail. Section IV presents the experimental results. Section V discusses the results and provides hints at plausible future research lines. Finally, Section VI concludes this article with some remarks.

II. Related Works

In this section, we review the existing literature on LULC classification and urban flood detection using crowdsourced and remote sensing data.

A. LULC Classification Using Crowdsourced Data

Crowdsourcing is increasingly recognized as a valuable source for understanding various human and land activities [20]. New emerging types of crowdsourced data provide complementary information for LULC classification, including geotagged photos, social media data, traffic trajectories, points of interest (POIs), and volunteered geographic information [31]. In general, crowdsourced data are served as ground truth and training samples to obtain LULC information. For example, Schultz et al. [32] combined OSM tags and remote sensing data for LULC classification in Heidelberg, Germany. Fritz et al. [33] described the global LULC reference data collected by a crowdsourcing platform called Geo-Wiki, which provided information on land cover disagreement and human impact. Andrade et al. [34] investigated the potential of POI data to characterize geographic spaces, and presented an approach for LULC classification based on different types of features extracted from POIs.

B. Flood Detection Using Remote Sensing Data

Remote sensing technology enables large-scale observations of urban floods in an objective manner. Common data sources include optical remote sensing satellites and SAR data. Data from optical remote sensing satellites, such as MODIS, Sentinel-2, and Landsat Thematic Mapper, Enhanced Thematic Mapper Plus, and Operational Land Imager, can provide rich spectral information [35], [36], [37]. Based on the difference in spectral reflectance of the flooded areas, the contrast between the flooded areas and other land surfaces is enhanced for flood detection. For example, Samela et al. [38] combined spectral indices, such as modified normalized difference water index (NDWI), NDWI, and normalized difference turbidity index, calculated from Sentinel-2 images and digital elevation models to enhance real-time identification of river flooding. Tulbure et al. [39] applied machine learning to detect surface water and flooding dynamics based on the Harmonized Landsat Sentinel-2 surface reflectance product of the National Aeronautics and Space Administration, which combines Landsat-8 and Sentinel-2 observations with high temporal frequency of 3–4 days.

SAR data provided by instruments can break through the limitations of severe weather conditions, such as clouds and rain, during Earth observation, and provide large-scale spatial data for urban flood detection during disaster periods, such as Sentinel-1, TerraSAR-X, and Advanced Land Observing Satellite-2/Phased Array L-band SAR-2 [40], [41], [42]. For instance, Islam and Meng [43] designed threshold, change detection, unsupervised, and supervised classification methods for urban flood mapping according to different combinations of Sentinel-1 transmit-horizontal receive and vertical transmit-vertical receive (VV) polarizations. Baghermanesh et al. [44] integrated simulated reflectivity maps and polarimetric and interferometric features generated from TerraSAR-X images to improve urban flood detection. Based on existing research, a new method is developed for fine-grained flood detection in complex urban environments by integrating crowdsourced and remote sensing data, and a case study is provided for testing.

III. Materials and Methods

This section introduces the datasets and the proposed method for urban flood detection in detail (see Fig. 1). The input data include OSM data, finer resolution observation and monitoring of global land cover (FROM-GLC10) product [45], and Sentinel-1 SAR intensity and coherence. Based on the integration of these data, fine-grained flood detection in complex urban environments is realized.

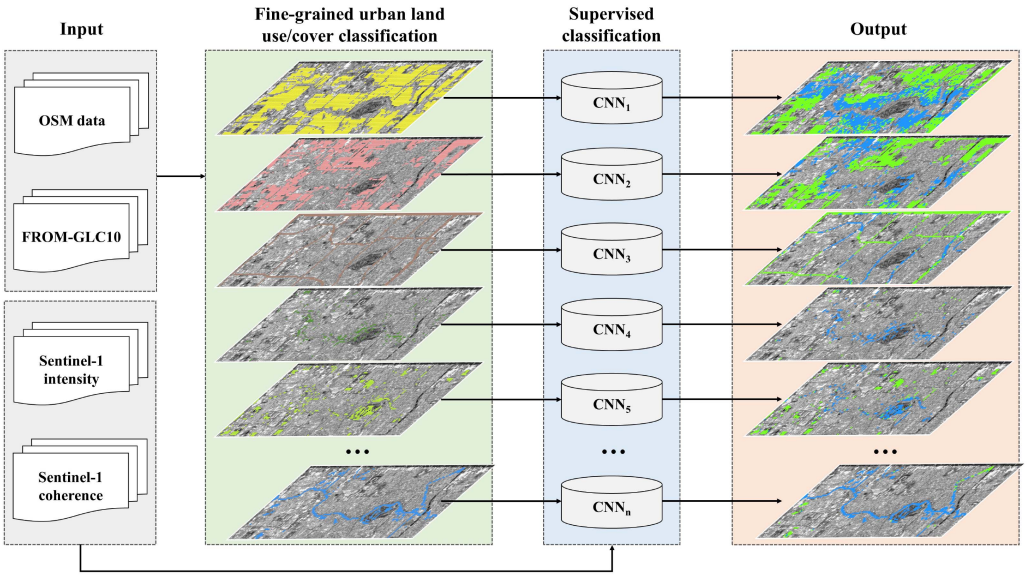

Fig. 1. Flowchart of fine-grained urban flood detection by combining OSM data, finer resolution observation and monitoring of global land cover (FROM-GLC10) product, Sentinel-1 SAR images, and CNNs.

A. Test Case

Hurricane Harvey made landfall in Texas on 25 August 2017, causing severe damages in large areas of Houston, the fourth largest city in the United States [46]. After hitting Houston, Harvey weakened to a tropical storm and progressed slowly, resulting in extremely high rainfall. According to the statistics by local National Weather Service office in Houston, 370 and 408 mm of daily rainfall were observed on 26 and 27 August, respectively. As a result, the Houston bayous burst their banks for several days, leading to widespread catastrophic flooding. Taking the 2017 Houston flood event as a test case, two areas located in western Houston are considered, which are mainly occupied by residential houses/apartments, commercial and industrial districts, parks, forest, grassland, reservoirs, and waterways. The spatial extent of the two study areas is shown in Figs. S1 and S2 in the Supplementary Material, respectively. Specifically, study area 1 is used to construct the training set, validation set, and test set required by the urban flood detection model. The trained classification model is directly applied to detect the urban floods in study area 2 for further test and analysis.

B. Sentinel-1 SAR Data

In response to the 2017 flood event in Houston, the pre-event and co-event ground range detected data and single look complex data of Sentinel-1 VV polarized interferometric wide swath mode were acquired from the Copernicus Open Access Hub.[2] Here, we generate the Sentinel-1 SAR intensity and coherence images using Sentinel application platform [47]. The intensity images are processed by orbit correction, thermal noise removal, radiation calibration, speckle reduction with the Refined Lee speckle filter (window size of 7 × 7 pixels), radiometric terrain correction, and conversion from linear to dB. The coherence images are processed by orbit correction, back geo-coding, coherence estimation with a window size of 28 × 7 (range × azimuth), debursting, terrain phase removal, multilooking (window size of 4 × 1 pixels), and resampling to 10-m resolution. Table I provides details about the exact acquisition dates of the involved Sentinel-1 intensity and coherence data.

TABLE I
SENTINEL-1 SAR INTENSITY AND COHERENCE DATA USED IN THE 2017 HOUSTON FLOOD EVENT

Type	Acquisition date	Resolution (m)
SAR intensity	24/08/2017	10
	30/08/2017	10
SAR coherence	18/08/2017–24/08/2017	10
	24/08/2017–30/08/2017	10

C. OSM Data

OSM is a collaborative project updated and maintained by a community of volunteers. OSM data can be accessed and downloaded for free through its official website.[3] Here, we collect OSM line vector data to support LULC classification in the studied areas, including road data and waterway data [see Figs. S1(a) and S2(a) in the Supplementary Material]. Specifically, we define four meta-categories of LULC based on OSM data: 1) residential areas, 2) service areas, 3) main roads, and 4) waterways. The tags in OSM to our meta-categories are as follows:

1) *residential areas:* using tag value "residential";
2) *service areas:* using tag value "service";

[2][Online]. Available: https://scihub.copernicus.eu/

[3][Online]. Available: http://www.openstreetmap.org

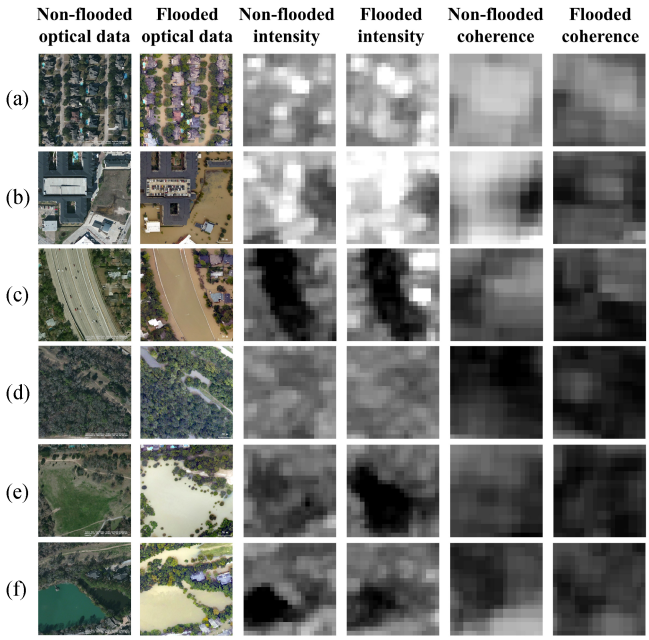

Fig. 2. Variations of Sentinel-1 SAR intensity and coherence for different LULC types under nonflooded and flooded conditions: (a) residential areas, (b) service areas, (c) main roads, (d) forest, (e) grassland, and (f) waterways.

3) *main roads:* using tag values "motorway," "trunk," primary, and secondary;
4) *waterways:* using tag values "drain," "river," and "stream."

D. FROM-GLC10 Product

FROM-GLC10 is the first 10-m resolution global land cover product, which is developed based on global Sentinel-2 images and powerful cloud computing capabilities of Google Earth Engine [45]. The FROM-GLC10 product divides land cover into ten types of cropland, forest, grassland, shrubland, tundra, wetland, water, impervious surface, bareland, and snow/ice, with an overall accuracy (OA) of 72.76% [45]. In this study, the FROM-GLC10 product is used to provide auxiliary information for fine-grained classification of urban LULC.

E. Ground-Truth Data

Based on the very high resolution aerial photographs acquired on 30–31 August 2017 by the National Oceanic and Atmospheric Administration Remote Sensing Division, we virtually digitize the ground-truth flooded and nonflooded areas with a spatial resolution of 70 m in the study areas [see Figs. S1(b) and S2(b) in the Supplementary Material].

F. SAR Intensity and Coherence in Urban Environments

There are various flooded/nonflooded reflection/scattering mechanisms in complex urban environments. Here, we analyze the variations of Sentinel-1 SAR intensity (σ°) and coherence (γ) for different LULC types under nonflooded and flooded conditions, including residential areas, service areas, main roads, forest, grassland, and waterways (see Fig. 2). Residential areas are described as a mixture of impervious surfaces and vegetation [see Fig. 2(a)]. A dihedral corner reflector formed from the wall–ground structure causes double bounce effect in residential areas, and the floods have a higher dielectric constant, resulting in an increase in σ° [48], [49]. In addition, the impervious surfaces (e.g., houses/apartments) are steady targets characterized by high γ, while the floods between buildings can cause a significant decrease of the γ. Compared with residential areas, service areas have a higher proportion of impervious surface and a lower proportion of vegetation [see Fig. 2(b)]. Flooded service areas show a larger increase in σ° and a larger decrease in γ. Main roads includes motorways, trunks, primary roads, and secondary roads, which are smooth in both flooded and nonflooded conditions [see Fig. 2(c)]. In this case, backscattered energy is predominantly directed in the specular direction, causing low σ° [12]. Meanwhile, the floods on the main roads can cause a decrease in γ. As for forest, the presence of floods between sparse trees can increase σ° by means of the double bounce effect, but tree canopies may also block dihedral scattering [see Fig. 2(d)]. Due to the low correlation of vegetation and the decorrelation of floods [13], both flooded and nonflooded forests show low γ. When grassland is flooded, the surface backscatter changes to specular reflection [12], causing a significant decrease in σ° [see Fig. 2(e)]. The γ of flooded grassland can decrease due to the changes in the spatial distribution of scatterers. The changes of σ° and γ in waterways are mainly influenced by the surrounding land cover [see Fig. 2(f)]. For instance, dihedral scattering between floods and trees will increase σ° and floods can lead to a certain degree of γ decline. Note that mixed pixels of medium-resolution images and frequent human activities can also lead to changes in the composition and position of scatterers, which makes the reflection/scattering characteristics of LULC more complicated in urban areas [12], [13], [50].

G. Fine-Grained LULC Classification Using OSM Data

Citizen science/crowdsourcing has shown great potential for urban LULC classification. Based on the collected OSM line vector data, we generate the following meta-categories for fine-grained LULC classification of the study areas: residential areas, service areas, main roads, and waterways. First of all, the multitemporal Sentinel-1 intensity and coherence images (pre-event and co-event) are split into the nonoverlapping patches of spatial size 7×7. Since the spatial resolution of the Sentinel-1 images is 10 m, all patches cover a ground area of 70 m $\times$ 70 m. Assume that there are J LULC meta-categories; we calculate the length of each meta-category (length_j) in each image patch through spatial analysis. The LULC of the image patch i can be expressed as follows:

$$\text{LULC}_i = \{j | \max(\text{length}_j), j \in [1, J]\}. \quad (1)$$

With respect to the image patches that are not classified by (1), we combine the FROM-GLC10 product for subsequent classification. Assume that there are K land cover types of the FROM-GLC10 data in the study areas; we calculate the area of the kth type (area_k) in each unclassified i image patch through spatial statistics. On this basis, the LULC of the unclassified

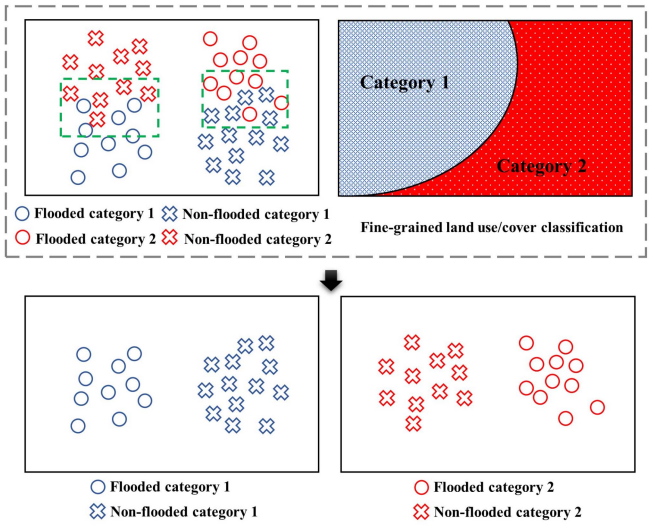

Fig. 3. Graphical illustration of processing similar reflection/scattering characteristics of different LULCs under flooded and nonflooded conditions by using fine-grained LULC classification obtained from OSM data.

image patch i is given as follows:

$$\text{LULC}_i = \{k|\max(\text{area}_k), k \in [1, K]\}. \quad (2)$$

Note that, for the land cover types that do not exist in the meta-categories obtained from the OSM data, these types of FROM-GLC10 are supplemented for LULC classification, such as forest and grassland. For the land cover types similar to meta-categories, these types are reclassified into the meta-categories. For example, the types of water and wetland of FROM-GLC10 are reclassified into waterways. The impervious surface type of FROM-GLC10 is reclassified into residential areas or service areas or main roads in the meta-categories, depending on the number of meta-categories within 3×3 image patches.

H. Urban Flood Detection by Integrating Multisource Data

The fine-grained LULC classification obtained through OSM data provides a solution to the issue that a flooded LULC may have similar reflection/scattering characteristics than another nonflooded LULC in a complex urban environment (see Fig. 3). It can be observed in the graph that there are two categories of LULC with similar reflection/scattering similar characteristics under flooded and nonflooded conditions. As marked by the green dotted rectangles, it is very difficult to separate flooded and nonflooded areas. Combining the fine-grained classification of these two LULC categories, it is much easier to classify the flooded and nonflooded category 1, and reduce the possibility of misclassification. The same is true for category 2.

Convolutional neural networks (CNNs) can automatically learn complex, nonlinear relationships between input features and output targets, and are widely used in urban flood detection [41]. Based on the information of fine-grained LULC classification, we adopt CNNs to conduct patchwise urban flood detection for each LULC type. Compared with pixelwise classification models, patchwise models can reduce the impact of errors in multisequential image registration, and save time and cost for annotation in urban areas with complex backscattering backgrounds [51]. Specifically, the labeled flooded and nonflooded patches of each LULC type in study area 1 are, respectively, divided into training dataset, validation dataset, and test dataset, according to a ratio 6:2:2. In this study, we use a simple five-layer CNN model for the flood detection of each LULC, consisting of one input layer, three hidden layers and one output layer. The hidden layers, respectively, contain 32, 64, 128 neuron nodes, using the ReLU activation function [52]. The input data include pre-event Sentinel-1 SAR intensity and coherence, and co-event Sentinel-1 SAR intensity and coherence. Each CNN model is trained with a batch size of 64, using Adam optimizer with an initial learning rate of $1e^{-4}$ and momentum parameters $(\beta_1, \beta_2) = (0.9, 0.999)$. The number of epochs for model training is set to 200. Instead of using early stopping, the model weights are saved every ten epochs and the best model is selected for testing. Besides the test dataset, we directly apply the trained CNN models for flood detection in study area 2 to verify the effectiveness of the proposed method.

I. Accuracy Assessment of Urban Flood Detection

Here, we compare the results of urban flood detection obtained by different methods with ground-truth flooded areas for accuracy assessment. The quantitative metrics of precision: recall, F1 score, OA, and Cohen's Kappa coefficient are calculated by combining the confusion matrix. For comparative analysis, we implement the following two baseline experiments: 1) *"CNN":* multiple training datasets, validation datasets, and test datasets of different LULC types are combined into one training dataset, validation dataset, and test dataset, which are used for urban flood detection through a patchwise CNN model and 2) *"FROM-GLC10":* we only use the FROM-GLC10 product for land cover classification, and patchwise CNN models are trained for each land cover type.

IV. Results

In this section, we first present the results of fine-grained LULC classification obtained through OSM data. Then, we quantitatively evaluate the results of urban flood detection generated by different methods.

A. Fine-Grained Urban LULC Classification

Combining the OSM line vector data and the FROM-GLC10 product, we generate the fine-grained urban LULC classification maps in the study areas (see Fig. 4, and Fig. S3 in the Supplementary Material). The study areas contain a total of six urban LULC types, namely, residential areas, service areas, main roads, forest, grassland, and waterways. Residential areas and service areas are widely distributed in study area 1, accounting for 73.43% of the area. Main roads show obvious linear characteristics, with an area proportion of 10.94%. The area proportions of waterway, grassland, and forest are 6.57%, 6.19%, and 2.88%, respectively. In study area 2, residential areas are the most dominant LULC type, accounting for 53.79% of the area. The area proportions

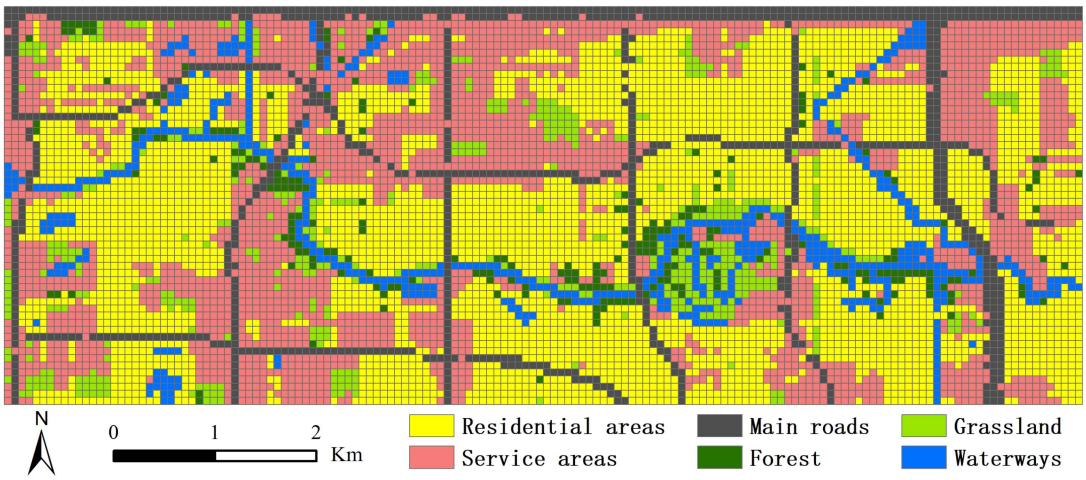

Fig. 4. Fine-grained classification of urban LULC in study area 1.

of forest, service areas, grassland, waterways, and main roads are 16.61%, 14.10%, 6.59%, 5.91%, and 2.98%, respectively.

B. Fine-Grained Urban Flood Detection

First of all, the red, green, and blue (RGB) band combination of multitemporal Sentinel-1 SAR intensity and coherence images in study area 1 is used for qualitative analysis to promote the understanding of the SAR reflection/backscattering mechanisms in a complex urban environment with flooded and nonflooded condition (see Fig. 5). Fig. 5(a) presents the RGB color composite given by R: pre-event intensity, and G and B: co-event intensity. Red color may indicate the flood bare soil or short vegetation with a decrease of SAR intensity. Cyan may be partially flooded residential areas or vegetation, and dihedral scattering with floods leads to an increase of SAR intensity. White color indicates flooded areas where dihedral scattering is dominant such as service areas. Fig. 5(b) presents the RGB color composite given by R: pre-event coherence, and G and B: co-event coherence. Darker areas indicate lower coherence in both pre-event and co-event, which generally consist of vegetation or areas with dense activities, such as parking lots and roads. White color represents the nonflooded built-up areas that have high coherence in the pre-event and co-event. Red color may be the zones where built-up areas are decorrelated by floods or vegetation is decorrelated by random changes. Fig. 5(c) presents the RGB color composite given by R: co-event intensity, G: pre-event coherence, and B: co-event coherence. Yellow color indicates the flooded built-up areas, such as service areas. Brown color may be the areas of mixed flooded buildings and vegetation, such as residential areas. White and cyan colors are the nonflooded built-up areas. Red color represents the flooded or nonflooded vegetation with medium SAR intensity and low SAR coherence.

Based on the obtained fine-grained LULC classification, we, respectively, train CNN models for each LULC type for urban flood detection. Table II gives the flood detection results of various LULC types on the test datasets. The OAs of residential areas, service areas, main roads, forest, grassland, and waterways

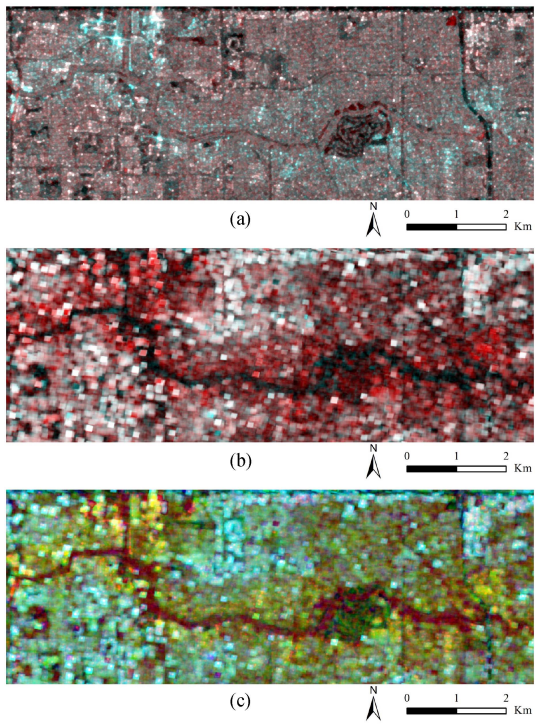

Fig. 5. RGB color composites of multitemporal Sentinel-1 SAR intensity and coherence images for the interpretation of different LULCs under flooded and nonflooded conditions. (a) R = σ° (2017/08/24), B= σ° (2017/08/30), B= σ° (2017/08/30). (b) γ (2017/08/18-2017/08/24), G = γ (2017/08/24-2017/08.30), B= γ (2017/08/24-2017/08/30). (c) R = σ° (2017/08/30), G = γ (2017/08/18-2017/08/24), B = γ (2017/08/24-2017/08/30).

are 0.8, 0.89, 0.85, 0.92, 0.82, and 0.92, respectively. The overall results of the proposed method can be obtained by combining the flood detection results of each LULC type (see Table III). It can found that the proposed method performs more prominently than the baseline methods according to all quantitative metrics. Compared with the baseline method "CNN," F1 score, OA, and Kappa of our method increase by 2.57%, 2.35%, and 4.74%, respectively. This indicates that the similar reflection/scattering

TABLE II
EVALUATION OF THE FLOOD DETECTION RESULTS OF VARIOUS LULC TYPES ON THE TEST DATASET OBTAINED BY THE PROPOSED METHOD

Types	Precision	Recall	F1	OA	Kappa
Residential areas	0.8630	0.7000	0.7730	0.8027	0.6018
Service areas	0.8720	0.7267	0.7927	0.8860	0.7150
Main roads	0.8222	0.6491	0.7255	0.8495	0.6238
Forest	0.9302	0.9756	0.9524	0.9200	0.7033
Grassland	0.8085	0.7917	0.8000	0.8190	0.6348
Waterways	0.9223	0.9896	0.9548	0.9196	0.5987

TABLE III
EVALUATION OF THE FLOOD DETECTION RESULTS OBTAINED BY DIFFERENT METHODS ON THE TEST SET

Methods	Precision	Recall	F1	OA	Kappa
CNN	0.8321	0.7447	0.7860	0.8209	0.6328
FROM-GLC10	0.8206	0.7460	0.7815	0.8164	0.6238
Proposed	**0.8718**	**0.7593**	**0.8117**	**0.8444**	**0.6802**

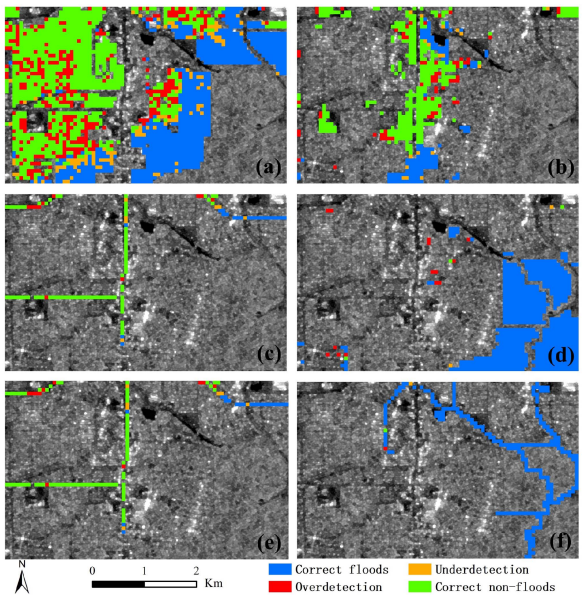

Fig. 6. Flood detection results of various LULC types in study area 2 obtained by the proposed method.

characteristics between flooded and nonflooded LULCs can be well separated by our method.

To further test the effectiveness of the proposed method, the CNN models trained in the study area 1 are directly applied to study area 2 for urban flood detection (see Fig. 6). As given in Table IV, the OAs of residential areas, service areas, main roads, forest, grassland, and waterways are 0.78, 0.85, 0.84, 0.97, 0.65, and 0.99, respectively. Similarly, the flood detection results in the entire study area 2 can be obtained by combining the corresponding results of each LULC type [see Table V and Fig. 7(c)]. Compared with the baseline methods, the F1 score, OA, and Kappa of our method increase by more than 3.96%, 4.53%, and 9.26%, respectively. It can also be found that more areas of flood

TABLE IV
EVALUATION OF THE FLOOD DETECTION RESULTS OF VARIOUS LULC TYPES IN STUDY AREA 2 OBTAINED BY THE PROPOSED METHOD

Types	Precision	Recall	F1	OA	Kappa
Residential areas	0.6861	0.8615	0.7639	0.7811	0.5647
Service areas	0.6667	0.8784	0.7580	0.8460	0.6482
Main roads	0.6563	0.7500	0.7000	0.8421	0.5935
Forest	0.9778	0.9968	0.9872	0.9748	0.2638
Grassland	0.6000	0.8780	0.7129	0.6548	0.3165
Waterways	0.9955	0.9955	0.9955	0.9912	0.4955

TABLE V
EVALUATION OF THE FLOOD DETECTION RESULTS OBTAINED BY DIFFERENT METHODS IN STUDY AREA 2

Methods	Precision	Recall	F1	OA	Kappa
CNN	0.7707	0.8494	0.8081	0.7904	0.5784
FROM-GLC10	0.7300	0.9231	0.8153	0.7831	0.5612
Proposed	**0.7864**	0.9194	**0.8477**	**0.8284**	**0.6538**

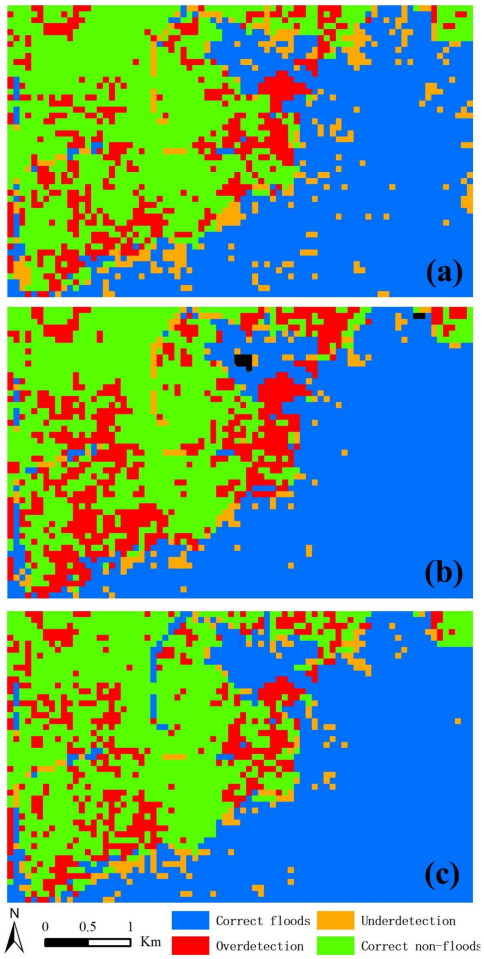

Fig. 7. Detection results of flooded extents in study area 2 obtained by (a) CNN, (b) FROM-GLC10, and (c) the proposed method.

underdetection occur when using the baseline method "CNN" [see Fig. 7(a)], while more areas of overdetection occur when using the baseline method "FROM-GLC10" [see Fig. 7(b)].

V. Discussion

In this article, we develop a new method for fine-grained and accurate flood detection by integrating multitemporal Sentinel-1 SAR and OSM data. Different from previous studies [53], [54], the proposed method leverages LULC information to improve urban flood detection, instead of overlapping LULC after flood detection for damage assessment. Based on the fine-grained LULC classification, the issue that similar reflection/scattering characteristics between flooded and nonflooded LULC in complex urban environment can be addressed according to the results obtained by our method and the baseline method "CNN" (see Tables III and V). In addition, similar results obtained by two baseline methods indicate the importance of fine-grained and accurate classification of urban LULC. Specifically, there are only three land cover types obtained by "FROM-GLC10", i.e., imperious surface, forest, and grassland, and many patches that mix vegetation and buildings may be misclassified as forest. Therefore, the baseline method "FROM-GLC10" does not achieve as good performance as our method in the context of urban flood detection.

So far, flood detection in complex urban environments has been a very challenging task [12], [50]. In future research, besides the OSM line vector data used in this study, other OSM data that have been evaluated for spatial coverage, land attributes, and spatio–temporal positioning accuracy [29], [55], [56] can also be considered to further improve the fine-grained urban LULC classification. In addition, the proposed method may be limited by sample size during model training, especially for the LULC types with smaller areas. Therefore, data augmentation can be used to generate more data and improve the generalization ability of the classification models [57], [58].

VI. Conclusion

There are similar reflection/scattering characteristics between flooded and nonflooded LULCs in complex urban environments. To address this issue, a new method for fine-grained and accurate flood detection is proposed by integrating multitemporal Sentinel-1 SAR images and OSM line vector data. Taking the 2017 Houston flood event as a test case, we, respectively, train CNN models for each LULC type to detect urban flood extents. According to our experiments, the proposed method performs more prominently than the baseline methods in the task of flood detection. In addition, our method can separate similar reflection/scattering characteristics between flooded and nonflooded LULCs to improve urban flood detection.

References

[1] P. J. Ward et al., "A global framework for future costs and benefits of river-flood protection in urban areas," *Nature Climate Change*, vol. 7, no. 9, pp. 642–646, 2017.

[2] W. Cao, Y. Zhou, B. Güneralp, X. Li, K. Zhao, and H. Zhang, "Increasing global urban exposure to flooding: An analysis of long-term annual dynamics," *Sci. Total Environ.*, vol. 817, 2022, Art. no. 153012.

[3] B. Tellman et al., "Satellite imaging reveals increased proportion of population exposed to floods," *Nature*, vol. 596, no. 7870, pp. 80–86, 2021.

[4] E. C. O'Donnell and C. R. Thorne, "Drivers of future urban flood risk," *Philos. Trans. Roy. Soc. A*, vol. 378, no. 2168, 2020, Art. no. 20190216.

[5] W. Zhu et al., "Urban flood-related remote sensing: Research trends, gaps and opportunities," *Remote Sens.*, vol. 14, no. 21, 2022, Art. no. 5505.

[6] Z. Liu, Q. Qiu, J. Li, L. Wang, and A. Plaza, "Geographic optimal transport for heterogeneous data: Fusing remote sensing and social media," *IEEE Trans. Geosci. Remote Sens.*, vol. 59, no. 8, pp. 6935–6945, Aug. 2021.

[7] A. Teodoro and L. Duarte, "The synergy of remote sensing and geographical information systems in the management of natural disasters," in *Nanotechnology-Based Smart Remote Sensing Networks for Disaster Prevention*. Amsterdam, The Netherlands: Elsevier, 2022, pp. 217–230.

[8] M. R. Atefi and H. Miura, "Detection of flash flood inundated areas using relative difference in NDVI from Sentinel-2 images: A case study of the Aug. 2020 event in Charikar, Afghanistan," *Remote Sens.*, vol. 14, no. 15, 2022, Art. no. 3647.

[9] A. D'Addabbo, A. Refice, G. Pasquariello, F. P. Lovergine, D. Capolongo, and S. Manfreda, "A Bayesian network for flood detection combining SAR imagery and ancillary data," *IEEE Trans. Geosci. Remote Sens.*, vol. 54, no. 6, pp. 3612–3625, Jun. 2016.

[10] E. Hamidi, B. G. Peter, D. F. Muñoz, H. Moftakhari, and H. Moradkhani, "Fast flood extent monitoring with SAR change detection using Google Earth Engine," *IEEE Trans. Geosci. Remote Sens.*, vol. 61, Jan. 2023, Art. no. 4201419.

[11] L. Landuyt, F. M. Van Coillie, B. Vogels, J. Dewelde, and N. E. Verhoest, "Towards operational flood monitoring in flanders using Sentinel-1," *IEEE J. Sel. Topics Appl. Earth Observ. Remote Sens.*, vol. 14, pp. 11004–11018, Oct. 2021.

[12] Y. Li, S. Martinis, and M. Wieland, "Urban flood mapping with an active self-learning convolutional neural network based on TerraSAR-X intensity and interferometric coherence," *ISPRS J. Photogrammetry Remote Sens.*, vol. 152, pp. 178–191, 2019.

[13] M. Chini, R. Pelich, L. Pulvirenti, N. Pierdicca, R. Hostache, and P. Matgen, "Sentinel-1 ISAR coherence to detect floodwater in urban areas: Houston and hurricane Harvey as a test case," *Remote Sens.*, vol. 11, no. 2, 2019, Art. no. 107.

[14] D. Weydahl, "Analysis of ERS SAR coherence images acquired over vegetated areas and urban features," *Int. J. Remote Sens.*, vol. 22, no. 14, pp. 2811–2830, 2001.

[15] X. Liang, Y. Lin, and H. Zhang, "Mapping urban impervious surface with an unsupervised approach using interferometric coherence of SAR images," *IEEE J. Sel. Topics Appl. Earth Observ. Remote Sens.*, vol. 15, pp. 2734–2744, Feb. 2022.

[16] Y. Wang, Y. Sun, X. Cao, Y. Wang, W. Zhang, and X. Cheng, "A review of regional and global scale land use/land cover (LULC) mapping products generated from satellite remote sensing," *ISPRS J. Photogrammetry Remote Sens.*, vol. 206, pp. 311–334, Dec. 2023.

[17] P. A. Tavares, N. E. S. Beltrão, U. S. Guimarães, and A. C. Teodoro, "Integration of Sentinel-1 and Sentinel-2 for classification and LULC mapping in the urban area of Belém, eastern Brazilian Amazon," *Sensors*, vol. 19, no. 5, 2019, Art. no. 1140.

[18] X. Huang, W. Yuan, J. Li, and L. Zhang, "A new building extraction postprocessing framework for high-spatial-resolution remote-sensing imagery," *IEEE J. Sel. Topics Appl. Earth Observ. Remote Sens.*, vol. 10, no. 2, pp. 654–668, Feb. 2017.

[19] W. Zhang, W. Li, C. Zhang, D. M. Hanink, X. Li, and W. Wang, "Parcel-based urban land use classification in megacity using airborne LiDAR, high resolution orthoimagery, and Google street view," *Comput. Environ. Urban Syst.*, vol. 64, pp. 215–228, 2017.

[20] J. Li, Z. Liu, X. Lei, and L. Wang, "Distributed fusion of heterogeneous remote sensing and social media data: A review and new developments," *Proc. IEEE*, vol. 109, no. 8, pp. 1350–1363, Aug. 2021.

[21] C. C. Fonte, J. A. Patriarca, M. Minghini, V. Antoniou, L. See, and M. A. Brovelli, "Using OpenStreetMap to create land use and land cover maps: Development of an application," in *Proc. Geospatial Intell.: Concepts, Methodol., Tools, Appl. IGI Glob.*, 2019, pp. 1100–1123.

[22] I. Moorthy, S. Fritz, L. See, and I. McCallum, "LandSense: A citizen observatory and innovation marketplace for land use and land cover monitoring," in *Proc. EGU Gen. Assem. Conf. Abstr.*, 2017, Art. no. 8562.

[23] L. See et al., "Generating WUDAPT's specific scale-dependent urban modeling and activity parameters: Collection of level 1 and level 2 data," in *Proc. 9th Int. Conf. Urban Climate, 12th Symp. Urban Environ.*, Toulouse, France, 2015.
[24] B. A. Johnson and K. Iizuka, "Integrating OpenStreetMap crowdsourced data and Landsat time-series imagery for rapid land use/land cover (LULC) mapping: Case study of the Laguna de Bay area of the Philippines," *Appl. Geogr.*, vol. 67, pp. 140–149, 2016.
[25] P. Mooney and P. Corcoran, "Analysis of interaction and co-editing patterns amongst OpenStreetMap contributors," *Trans. GIS*, vol. 18, no. 5, pp. 633–659, 2014.
[26] M. Haklay, "How good is volunteered geographical information? A comparative study of OpenStreetMap and ordnance survey datasets," *Environ. Plan. B: Plan. Des.*, vol. 37, no. 4, pp. 682–703, 2010.
[27] J. Jokar Arsanjani, P. Mooney, A. Zipf, and A. Schauss, "Quality assessment of the contributed land use information from OpenStreetMap versus authoritative datasets," *OpenStreetMap Giscience: Experiences, Res., Appl.*, pp. 37–58, 2015. [Online]. Available: https://link.springer.com/chapter/10.1007/978-3-319-14280-7_3#citeas
[28] R. Hecht, C. Kunze, and S. Hahmann, "Measuring completeness of building footprints in OpenStreetMap over space and time," *ISPRS Int. J. Geo-Inf.*, vol. 2, no. 4, pp. 1066–1091, 2013.
[29] S. S. Sehra, J. Singh, and H. S. Rai, "A systematic study of OpenStreetMap data quality assessment," in *Proc. 11th Int. Conf. Inf. technol.: New Gener.*, 2014, pp. 377–381.
[30] M. Haklay and P. Weber, "OpenStreetMap: User-generated street maps," *IEEE Pervasive Comput.*, vol. 7, no. 4, pp. 12–18, Oct.-Dec. 2008.
[31] H. Wu, Z. Gui, and Z. Yang, "Geospatial Big Data for urban planning and urban management," *Geo-Spatial Inf. Sci.*, vol. 23, pp. 273–274, 2020.
[32] M. Schultz, J. Voss, M. Auer, S. Carter, and A. Zipf, "Open land cover from OpenStreetMap and remote sensing," *Int. J. Appl. Earth Observ. Geoinformation*, vol. 63, pp. 206–213, 2017.
[33] S. Fritz et al., "A global dataset of crowdsourced land cover and land use reference data," *Sci. Data*, vol. 4, no. 1, pp. 1–8, 2017.
[34] R. Andrade, A. Alves, and C. Bento, "POI mining for land use classification: A case study," *ISPRS Int. J. Geo- Inf.*, vol. 9, no. 9, 2020, Art. no. 493.
[35] Q. Zhang, P. Zhang, and X. Hu, "Unsupervised GRNN flood mapping approach combined with uncertainty analysis using bi-temporal Sentinel-2 MSI imageries," *Int. J. Digit. Earth*, vol. 14, no. 11, pp. 1561–1581, 2021.
[36] A. Aggarwal, F. Rafique, E. Rajesh, and S. Ahmed, "Urban flood hazard mapping using change detection on wetness transformed images," *Hydrological Sci. J.*, vol. 61, no. 5, pp. 816–825, 2016.
[37] D. Sun, Y. Yu, and M. D. Goldberg, "Deriving water fraction and flood maps from MODIS images using a decision tree approach," *IEEE J. Sel. Topics Appl. Earth Observ. Remote Sens.*, vol. 4, no. 4, pp. 814–825, Dec. 2011.
[38] C. Samela, R. Coluzzi, V. Imbrenda, S. Manfreda, and M. Lanfredi, "Satellite flood detection integrating hydrogeomorphic and spectral indices," *Giscience Remote Sens.*, vol. 59, no. 1, pp. 1997–2018, 2022.
[39] M. G. Tulbure et al., "Can we detect more ephemeral floods with higher density harmonized Landsat Sentinel 2 data compared to Landsat 8 alone?," *ISPRS J. Photogrammetry Remote Sens.*, vol. 185, pp. 232–246, 2022.
[40] T. Bangira, L. Iannini, M. Menenti, A. Van Niekerk, and Z. Vekerdy, "Flood extent mapping in the Caprivi floodplain using Sentinel-1 time series," *IEEE J. Sel. Topics Appl. Earth Observ. Remote Sens.*, vol. 14, pp. 5667–5683, May 2021.
[41] I. Riyanto, M. Rizkinia, R. Arief, and D. Sudiana, "Three-dimensional convolutional neural network on multi-temporal synthetic aperture radar images for urban flood potential mapping in Jakarta," *Appl. Sci.*, vol. 12, no. 3, 2022, Art. no. 1679.
[42] H. Gokon, F. Endo, and S. Koshimura, "Detecting urban floods with small and large scale analysis of ALOS-2/PALSAR-2 data," *Remote Sens.*, vol. 15, no. 2, 2023, Art. no. 532.
[43] M. T. Islam and Q. Meng, "An exploratory study of Sentinel-1 SAR for rapid urban flood mapping on Google Earth Engine," *Int. J. Appl. Earth Observ. Geoinformation*, vol. 113, 2022, Art. no. 103002.
[44] S. S. Baghermanesh, S. Jabari, and H. McGrath, "Urban flood detection using TerraSAR-X and SAR simulated reflectivity maps," *Remote Sens.*, vol. 14, no. 23, 2022, Art. no. 6154.
[45] P. Gong et al., "Stable classification with limited sample: Transferring a 30-m resolution sample set collected in 2015 to mapping 10-m resolution global land cover in 2017," *Sci. Bull.*, vol. 64, no. 6, pp. 370–373, 2019.
[46] W. Zhang, G. Villarini, G. A. Vecchi, and J. A. Smith, "Urbanization exacerbated the rainfall and flooding caused by hurricane Harvey in Houston," *Nature*, vol. 563, no. 7731, pp. 384–388, 2018.
[47] M. Zuhlke et al., "SNAP (Sentinel application platform) and the ESA Sentinel 3 toolbox," in *Sentinel-3 Sci. Workshop*, vol. 734, 2015, Art. no. 21.
[48] D. Amitrano et al., "Urban areas enhancement in multitemporal SAR RGB images using adaptive coherence window and texture information," *IEEE J. Sel. Topics Appl. Earth Observ. Remote Sens.*, vol. 9, no. 8, pp. 3740–3752, 2016.
[49] G. Franceschetti, A. Iodice, and D. Riccio, "A canonical problem in electromagnetic backscattering from buildings," *IEEE Trans. Geosci. Remote Sens.*, vol. 40, no. 8, pp. 1787–1801, Aug. 2002.
[50] Y. Li, S. Martinis, M. Wieland, S. Schlaffer, and R. Natsuaki, "Urban flood mapping using SAR intensity and interferometric coherence via Bayesian network fusion," *Remote Sens.*, vol. 11, no. 19, 2019, Art. no. 2231.
[51] B. Peng, Z. Meng, Q. Huang, and C. Wang, "Patch similarity convolutional neural network for urban flood extent mapping using bi-temporal satellite multispectral imagery," *Remote Sens.*, vol. 11, no. 21, 2019, Art. no. 2492.
[52] X. Glorot, A. Bordes, and Y. Bengio, "Deep sparse rectifier neural networks," in *Proc. Int. Conf. Artif. Intell. Statist. JMLR Workshop Conf.*, 2011, pp. 315–323.
[53] K. Uddin, M. A. Matin, and F. J. Meyer, "Operational flood mapping using multi-temporal Sentinel-1 SAR images: A case study from Bangladesh," *Remote Sens.*, vol. 11, no. 13, 2019, Art. no. 1581.
[54] E. Psomiadis, K. X. Soulis, M. Zoka, and N. Dercas, "Synergistic approach of remote sensing and GIS techniques for flash-flood monitoring and damage assessment in Thessaly plain area, Greece," *Water*, vol. 11, no. 3, 2019, Art. no. 448.
[55] J. Kaur, J. Singh, S. S. Sehra, and H. S. Rai, "Systematic literature review of data quality within OpenStreetMap," in *Proc. IEEE Int. Conf. Next Gener. Comput. Inf. Syst.*, 2017, pp. 177–182.
[56] X. Xie, Y. Zhou, Y. Xu, Y. Hu, and C. Wu, "OpenStreetMMap data quality assessment via deep learning and remote sensing imagery," *IEEE Access*, vol. 7, pp. 176884–176895, 2019.
[57] S. Yang, W. Xiao, M. Zhang, S. Guo, J. Zhao, and F. Shen, "Image data augmentation for deep learning: A survey," 2022. [Online]. Available: https://arxiv.org/abs/2204.08610
[58] N. E. Khalifa, M. Loey, and S. Mirjalili, "A comprehensive survey of recent trends in deep learning for digital images augmentation," *Artif. Intell. Rev.*, vol. 55, pp. 2351–2377, 2022.

Zhenjie Liu (Member, IEEE) received the B.S. degree in land resource management and the M.E. degree in land use engineering from South China Agricultural University, Guangzhou, China, in 2016 and 2019, respectively, and the Ph.D. degree in geographic information systems from Sun Yat-sen University, Guangzhou, in 2023.

He is currently a Postdoc with the School of Computer Science, China University of Geosciences, Wuhan, China. His research interests include data fusion, deep learning, and urban flood mapping.

Jun Li (Fellow, IEEE) received the B.S. degree in geographic information systems from Hunan Normal University, Changsha, China, in 2004, the M.E. degree in remote sensing from Peking University, Beijing, China, in 2007, and the Ph.D. degree in electrical engineering from the Instituto de Telecomunicações, Instituto Superior Técnico, Universidade Técnica de Lisboa, Lisbon, Portugal, in 2011.

She is currently a Full Professor with the School of Computer Science, China University of Geosciences, Wuhan, China. Her main research interests include remotely sensed hyperspectral image analysis, signal processing, supervised and unsupervised learning, and active learning.

Dr. Li is the Editor-in-Chief of IEEE JOURNAL OF SELECTED TOPICS IN APPLIED EARTH OBSERVATIONS AND REMOTE SENSING. She has been a Guest Editor for several journals, including PROCEEDINGS OF IEEE and *ISPRS Journal of Photogrammetry and Remote Sensing*.

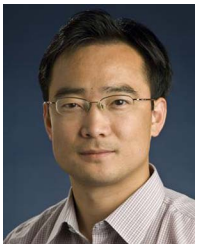

Lizhe Wang (Fellow, IEEE) received the B.E. and M.E. degrees in electrical engineering and automation from Tsinghua University, Beijing, China, in 1998 and 2001, respectively, and the D.E. degree (magna cumlaude) in applied computing science from the Karlsruhe Institute of Technology, Karlsruhe, Germany, in 2007.

He is currently with the Hubei Key Laboratory of Intelligent Geo-Information Processing and the School of Computer Science, China University of Geosciences, Wuhan, China. He is the Dean and "ChuTian" Chair Professor with the School of Computer Science, China University of Geosciences. His research interests include remote sensing data processing, digital Earth, and Big Data computing.

Dr. Wang is an Associate Editor for *Remote Sensing*, the *International Journal of Digital Earth*, ACM Computing Surveys, IEEE TRANSACTIONS ON PARALLEL AND DISTRIBUTED SYSTEMS, and IEEE TRANSACTIONS ON SUSTAINABLE COMPUTING. He is a Fellow of the Institution of Engineering and Technology and the British Computer Society. He was the recipient of Distinguished Young Scholars of the National Natural Science Foundation of China, National Leading Talents of Science and Technology Innovation, and 100-Talents Program of the Chinese Academy of Sciences.

Antonio Plaza (Fellow, IEEE) received the M.Sc. and Ph.D. degrees in computer engineering from the Department of Technology of Computers and Communications, University of Extremadura, Badajoz, Spain, in 1999 and 2002, respectively.

He is currently the Head of the Hyperspectral Computing Laboratory, Department of Technology of Computers and Communications, University of Extremadura, Cáceres, Spain. He has authored more than 430 journal articles, 25 book chapters, and 330 peer-reviewed conference proceeding articles. He has guest edited 17 special issues on hyperspectral remote sensing for different journals. He has reviewed more than 500 manuscripts for more than 50 different journals. His research interests include hyperspectral data processing and parallel computing of remote sensing data.

He was a member of the Editorial Board of IEEE GEOSCIENCE AND REMOTE SENSING NEWSLETTER from 2011 to 2012 and IEEE GEOSCIENCE AND REMOTE SENSING MAGAZINE in 2013. He is also a member of the Steering Committee of the IEEE JOURNAL OF SELECTED TOPICS IN APPLIED EARTH OBSERVATIONS AND REMOTE SENSING (JSTARS). He was a recipient of the recognition of Best Reviewers of IEEE GEOSCIENCE AND REMOTE SENSING LETTERS in 2009 and IEEE TRANSACTIONS ON GEOSCIENCE AND REMOTE SENSING in 2010, the Best Column Award of IEEE Signal Processing Magazine in 2015, the 2013 Best Paper Award of the JSTARS, the most highly cited paper in the Journal of Parallel and Distributed Computing from 2005 to 2010, and the best paper awards at the IEEE INTERNATIONAL CONFERENCE ON SPACE TECHNOLOGY and the IEEE SYMPOSIUM ON SIGNAL PROCESSING and Information Technology. He served as an Associate Editor for IEEE TRANSACTIONS ON GEOSCIENCE AND REMOTE SENSING. He is an Associate Editor of IEEE ACCESS. He served as the Director of Education Activities for the IEEE GEOSCIENCE AND REMOTE SENSING SOCIETY (GRSS) from 2011 to 2012, and as a President of the Spanish Chapter of IEEE GRSS from 2012 to 2016. He has been identified as a Highly Cited Researcher by Clarivate Analytics in 2018–2023.